

*Nano Lett.* Author manuscript; available in PMC 2013 October 29.

Published in final edited form as:

Nano Lett. 2008 July; 8(7): . doi:10.1021/nl801483w.

## Induction of Cell Polarization and Migration by a Gradient of Nanoscale Variations in Adhesive Ligand Spacing

Marco Arnold<sup>1,+</sup>, Vera C. Jakubick<sup>1,+</sup>, Theobald Lohmüller<sup>1</sup>, Patrick Heil<sup>1</sup>, Jacques Blümmel<sup>1</sup>, Elisabetta A. Cavalcanti-Adam<sup>1</sup>, Mónica López-García<sup>2</sup>, Paul Walther<sup>3</sup>, Horst Kessler<sup>2</sup>, Benjamin Geiger<sup>4</sup>, and Joachim P. Spatz<sup>1,\*</sup>

<sup>1</sup>Max Planck Institute for Metals Research, Dept. of New Materials and Biosystems; and University of Heidelberg, Dept. of Biophysical Chemistry, Postal Address: Heisenbergstr. 3, D-70569 Stuttgart, Germany

<sup>2</sup>Center of Integrated Protein Science Munich at the Technical University of Munich, Technical University of Munich, Department Chemie, Lichtenbergstrasse 4, D-85747 Garching, Germany

<sup>3</sup>University of Ulm, Central Unit for Electron Microscopy, Albert-Einstein-Allee 11, D-89069 Ulm, Germany

<sup>4</sup>Department of Molecular Cell Biology, Weizmann Institute of Science, Rehovot 76100, Israel

## **Abstract**

Cell interactions with adhesive surfaces play a vital role in the regulation of cell proliferation, viability and differentiation, and affect multiple biological processes. Since cell adhesion depends mainly on the nature and density of the adhesive ligand molecules, spatial molecular patterning, which enables the modulation of adhesion receptor clustering, might affect both the structural and signalling activities of the adhesive interaction. We herein show that cells plated on surfaces that present a molecularly defined spacing gradient of an integrin RGD ligand, can sense small but consistent differences in adhesive ligand spacing of about 1 nm across the cell diameter, which is approximately 61 µm when the spacing includes 70 nm. Consequently, these positional cues induce cell polarization, and initiate cell migration and signalling. We propose that differential positional clustering of the integrin transmembrane receptors is used by cells for exploring and interpreting their environment, at high spatial sensitivity.

Adhesion of tissue cells to the extracellular matrix depends on the activation of specific transmembrane receptors; e.g. integrins, which leads to the assembly of specialized adhesion sites known as focal adhesions (FA). Activation and spatial organization of integrins are mainly controlled by epitopes containing a RGD (R = arginine, G = glycine, D = aspartate) sequence, that are present on a variety of adhesive extracellular matrix (ECM) proteins. Recent studies indicated that beyond the chemical specificity of the adhesive epitope, many physical features of the adhesive surface, including its topography, rigidity, and precise epitope spacing, are critical for guiding receptor-mediated adhesion formation and signalling. Specifically, it was demonstrated that cyclic RGDfK peptides linked to nanogold particles which were arranged in pattern on substrates and interspaced by 58 or 73 nm, influence cell adhesion, spreading, focal adhesion assembly, and migration, in very different ways. In these studies, control experiments demonstrated that only the specific functionalization of nanogold particles with cyclic RGD induced integrin clustering and such focal adhesion formation upon interaction with cells such as 3T3-fibroblasts or –

Corresponding author: spatz@mf.mpg.de.

<sup>&</sup>lt;sup>+</sup>Both authors contributed equally to this work.

osteoblasts. Non-functionalized nanogold particles<sup>5</sup> or nanoparticles that were functionalized with a random sequence of amino acids, i.e. arginine, glycine, glutamic acid (RGE),<sup>9</sup> did not induce adhesion associated cell responses. Even more detailed, blocking of integrin v 3 by antibodies revealed no adhesion response if nanogold particle pattern were functionalized with cyclic RGD.<sup>8</sup>

The number of adhering cells, their morphology, and their alignment are affected by plating the cells on gradients of immobilized fibronectin<sup>10</sup> or RGD peptides.<sup>11</sup> Axon extensions of rat hippocampal neurons<sup>12</sup> and migrating cells<sup>13</sup> tend to preferentially orient towards increasing surface density of the corresponding adhesion molecules. However, despite compelling evidence from local directional cues, generated by variations in density of adhesion molecules, the mechanisms whereby cells sense these variations, as well as specific variations in density remain unclear.

In recent years, new tools for the generation of surfaces displaying adhesive ligand density gradients have been developed. These techniques include the photoimmobilization of peptides on self-assembled monolayers, <sup>14</sup> microfluidic systems, <sup>15</sup> contact printing, <sup>16</sup> or dippen lithography. <sup>17</sup> Gold nanoparticle density gradients may be obtained by assembling the nanoparticles along a concentration gradient of amino groups. <sup>18</sup> More recently, protein-coated gold and silver nanoparticles have been used for the assembly of protein density gradients, by varying the immersion time of the solid support. <sup>19</sup> On the molecular length scale, these methods enable quantification of an average molecular concentration, which gradually varies along the adhesive surface; however, they are too "noisy" to quantify the densities themselves, and density variations capable of inducing cell polarization.

We herein demonstrate a novel surface patterning technique for the generation of nanoparticle spacing gradients, which is based on controlled modulation of the self-assembly of diblock copolymer micelles. Due to the self-assembly of macromolecules, large-scale surface areas are easily processed by this technique. After successful biofunctionalization of the nanoparticles with c(-RGDfK-),<sup>5, 7, 8</sup> each single particle binds up to one integrin.<sup>20</sup> Upon adhesion of cells, the gradual increase in spacing between individual nanoparticles and thus, local changes in integrin clustering, enables the testing of the response sensitivity of cells to the spatial separation of individual adhesion molecules.

Block copolymer micelle nanolithography (BCMN) enables the positioning of 1-15 nm-sized gold particles in a quasi-hexagonal pattern, with a tunable particle spacing of 15-250 nm, by dip-coating a substrate, and subsequently subjecting it to a plasma process which removes the entire polymer but, at the same time, deposits gold particles on the substrate in well-defined patterns. <sup>21-24</sup> Varying the molecular weight of diblock copolymers causes variations in lateral spacing between the gold nanoparticles. Here, we demonstrate that the lateral spacing of gold nanoparticles also depends on the concentration of the micellar dipcoating solution and on the substrate retraction velocity, the latter of which enables the formation of well-defined nanoparticle spacing gradients.

Extended and highly regular monomicellar films were prepared by dip-coating Si(100)-wafers or glass cover slips into toluene solutions of Polystyrene(x)-*b*-Poly(2-vinylpyridine) (y) (PS(x)-*b*-P2VP(y)) diblock copolymers, as described in the Supplemental Material.

Scanning electron microscopy (SEM) was then used to evaluate particle spacing as a function of polymer concentration, revealing a particle spacing for the PS(1780)-*b*-P[2VP(HAuCl<sub>4</sub>)<sub>0.2</sub>](520) diblock copolymer which ranged from ~50 nm for 10 mg/mL, to ~170 nm for 0.1 mg/mL, when a substrate was retracted from the solution at a speed of 12 mm/min (Figure 1a). The graph displays a linear decrease in the particle spacing, as the polymer concentration increases from 1 to 5 mg/mL; this decrease saturates towards 50 nm

when the polymer concentration reaches 10 mg/mL. The insets in Fig. 1a depict two representative SEM micrographs, revealing quasi-hexagonal arrays of gold nanoparticles obtained at polymer concentrations of 1 mg/mL and 5 mg/mL.

The particle spacing was then varied by changing the substrate retraction velocity from 2.3 to 41.9 mm/min, using a 2 mg/mL solution of PS(1780)-b-P[2VP(HAuCl<sub>4</sub>)<sub>0.2</sub>](520) diblock copolymer. Increasing the retraction velocity led to a quasi-linear decrease in the particle spacing from approximately 125 to 95 nm (Fig. 1b). Notably, a maximal retraction velocity was also observed, above which the particle spacing saturates. This finding is explained by the observation that a faster retraction velocity of the substrate results in a thicker liquid film adsorbed to it, since the liquid has less time to flow back into the solution reservoir. This results in an increased number of deposited micelles per unit area, after evaporation of the solvent. Since a dissolved diblock copolymer micelle consists of a soft shell of polystyrene, micelles adjust to variations in micellar density during solvent evaporation by forming energetically favourable micellar core-to-core spacing, while each core positions the gold for deposition on substrates. Saturation of micellar packing is obtained when the polystyrene shell cannot be condensed any further.

A particle spacing gradient on one substrate was obtained by varying the substrate retraction velocity from the micellar solution. An extended range of particle spacing gradients was obtained by combining the alternation in polymer length with the retraction velocity (Fig. 1c). The combination of three different molecular weights of PS-P2VP diblock copolymers with different substrate retraction velocities yielded variations in particle spacing of between 80 and 250 nm. In general, a larger molecular weight of PS resulted in a wider particle spacing range by gradual variation of the substrate retraction velocity. Particle spacing gradients with different strengths of 19 +/- 1, 30 +/- 3 and 50 +/- 7 nm/mm were obtained by varying the acceleration of the retraction speed (Fig. 1d). The insets show SEM micrographs of highly regular gold nanopatterns at a substrate position below 3 mm and above 5 mm. Fig. 1e depicts particle spacing gradients of different directions on the same substrate.

The nanoparticle spacing gradients were applied to measure the sensitivity of adherent tissue cells to variations in spatial presentation of adhesive ligand "nanopatches", whereby each patch may bind up to one integrin molecule. Therefore, the substrate area which was not covered by gold nanoparticles was passivated by Polyethylene Glycol (PEG) to avoid nonspecific protein adsorption.<sup>5, 25</sup> The nanoparticles were functionalized with the c(RGDfK)thiol cell adhesive molecules, which specifically bind to integrins.<sup>5, 9</sup> Accordingly, each functionalized nanoparticle served as a c(-RGDfK-) adhesion patch. The patch size was approximately 8 nm; i.e., 6 nm diameter of the gold particle, plus a 2 nm layer formed by the c(-RGDfK-) layer. Therefore, each c(-RGDfK-) patch presented a single binding site for up to one integrin due to steric hindrance when cells were plated on the nanostructured support (Fig. 2a). <sup>20</sup> In former publications we demonstrated that non-functionalized nanogold particles<sup>5</sup> or particles that were functionalized with a peptide presenting a random chosen sequence, i.e. RGE, <sup>9</sup> did not induce any adhesion associated cell response. Even in the case of blocking the cell adhesion receptor integrin v 3 with antibodies but functionalizing the nanogold particle array with c(-RGDfK-) no adhesion of cells were found which proved the specificity of the surface functionalization concept once more. 8 The height of the nanoparticles was adjusted such that it matches the height of the PEG layer between the nanogold particles, i.e. ca. 6 nm. Thus, potential topographical effects did not account for cell adhesion associated response.<sup>5, 25</sup>Figure 2, b-d show high-resolution SEM micrographs which display cells' haptic sensitivity at the nanometer scale. Small cell protrusions of 10-20 nm are associated with single c(-RGDfK-) adhesion patches of 8 nm diameter.

The c(-RGDfK-) functionalized nanoparticle spacing gradient was applied to screen for changes in cellular morphology as a result of c(-RGDfK-) patch interspacing. The spacing between c(-RGDfK-) patches was continuously increased from  $\sim 50$  nm to  $\sim 80$  nm, between positions 3 mm and 5 mm of the substrate (Figure 2e) yielding a gradient strength of  $\sim 15$  nm/mm. High-magnification phase-contrast micrographs (Fig. 2e) indicate that the cell morphology changed from radial, well-spread adherent cells at a ligand patch spacing of  $\sim 50$  nm, to strongly elongated cells at a spacing of  $\sim 80$  nm.

The dynamic response of cells to a c(-RGDfK-) inter-particle spacing gradient was documented by analyzing the projected cell area after 2.5, 8 and 23 h in several substrate positions (Fig. 3a-c). After 2.5 h, most cells were round, and did not show a significant morphological variation along the gradient. The locally measured projected cell area was scattered around the mean projected cell area of 1500 µm<sup>2</sup>. Eight hours after plating, an increase in cell area along the gradient from ~1500 to ~2250 µm<sup>2</sup> for smaller patch spacing could be noted. After 23 h, position-dependent variations in cell spreading were clearly detected as a function of variations in spacing. On the dense part of the substrate, cells maintained a size of ~2250 µm<sup>2</sup>, while those attaching to c(-RGDfK-) inter-patch distances of 70 nm or more decreased their projected cell area even further, to a final size of ~1000 µm<sup>2</sup>. Undoubtedly, cells response was due to gradual variations in c(-RGDfK-) inter-patch distances since non-functionalized nanogold particles or particles that were functionalized with the RGE peptide did not at all indicate any comparable response (Fig. 3c). In general it was rather difficult to find cells which remain at the nanopattern substrates if the pattern was not functionalized with c(-RGDfK-). The couple of ten cells which were still discovered along the substrate were mainly spherical in shape and not spread. Evaluation of their mean projected cell area gave values below 250 µm<sup>2</sup> per cell (Fig. 3c). It is noteworthy that projected cell areas of spherical cell recall not their adhesion area. Even more, we claim that these couples of cells were attached to the substrates only due to defects in the substrate. In contrast, c(-RGDfK-) functionalization of the pattern obtained adhesion and spreading of couples of hundred cells with obviously much larger projected cell areas than in the other mentioned nanogold functionalization experiments. Only a slight linear decrease in the projected cell area was observed for spacing values which did not include a 70 nm distance; i.e., gradients ranging from 45 to 65 nm with a gradient strength of 40 nm/mm (Fig. 3d), or 80-110 nm with a gradient strength of 15 nm/mm (Fig. 3e).

Another morphometric parameter of adherent cells is the degree of cell polarization, obtained by calculating the Gradient Polarization Ratio (GPR), defined as the axial ratio of the most extended width of the cell body along the gradient (L<sub>x</sub>) and the most extended width of the cell body perpendicular to the gradient (L<sub>v</sub>) (Fig. 4a). In general, a GPR value of ~1 represents cells with no polarization, while a GPR > 1 indicates cells that are polarized. The GPR values are plotted here as a function of the substrate position. Within the error margins, the evaluated GPR values of MC3T3 osteoblasts at a homogeneous distributed ligand patch spacing of ~50 nm are constant, and show a typical value of ~1. The strongest polarization of cell bodies occurred in the middle of the gradient with a value of ~1.3, where the patch spacing range is between 60 and 70 nm. The orientation angle distribution of elongated cell bodies is given in Fig. 4b and c. In the case of a constant ligand patch spacing of 50 nm, cells did not choose a preferred orientation, even after 21 h. However, along the c(-RGDfK-) patch spacing gradient, cells polarized with a preferred angle, relative to the direction of the gradient, between 0 and 30°. Cell polarization was often accompanied by directional cell migration along the gradient. REF fibroblast migration tracks are plotted in Fig. 4d and e; approximately 15 different cells in each plot may be seen. While cells on a homogenous ligand patch spacing of ~60 nm navigated in all directions with the same probability, cells navigating on a ligand patch spacing gradient of

~ 25 nm/mm (covering 60 to 110 nm spacing) obviously sense the gradient, and migrate in the direction of smaller spacing (toward the left in Fig. 4e).

The weakest gradient to which cells responded had a strength of 15 nm/mm, if the gradient included the 70 nm spacing. Under these conditions, cells displayed an average length of  $<L_x>\sim61\pm3~\mu\text{m}$  in the direction of the gradient. A cell thus elongated along the gradient is exposed and can respond to a difference in ligand patch spacing of  $\sim0.9\pm0.5$  nm between the cell's front and rear. This sensitivity to such a small length scale is remarkable, being much smaller than the expected "noise", and is, most likely, achieved in a time-integrative manner. This sensitivity may only be realised with molecular operations such as optimal receptor clustering. One may speculate that this exquisite cellular sensitivity arises from conditions prevailing *in vivo*, such as the 67 nm periodicity given in collagen, which forms 80% of the environment of tissue cells.  $^{26}$  Therefore, our findings also address the precise conditions with which cellular environments must be constructed in order to sustain structure and function of living tissues.

In summary, the development of a novel nanoscale ligand spacing gradient enabled us to study the high sensitivity of tissue cells to changes in spatial presentation of adhesion ligand patches. Particle spacing gradients of varying strengths, and a spacing range covering 50 to 250 nm, was demonstrated with gold nanoparticles of approximately 6 nm in diameter. Specific biofunctionalization of the particle spacing gradient enabled us to determine the minimal gradient strength required in order to make cells polarise, i.e. 15 nm/mm gradient strength. Since each gold nanoparticle functionalized by c(-RGDfK-) peptides offers a single binding site for the adhesion receptor integrin, a gradual increase in particle spacing tests the importance of receptor clustering-based responses in the ability of cells to sense spatial variations of <1 nm, presented by the extracellular matrix.

## **Acknowledgments**

We wish to thank Thorsten Brach for technical assistance, Dr. Philippe Girard and Prof. Jennifer Curtis for writing the SEM Image Analysis program. The Landesstiftung Baden-Württemberg and the Max-Planck-Society are acknowledged for their financial support. This publication and the project described herein were also partly supported by the National Institutes of Health through the NIH Roadmap for Medical Research (PN2 EY 016586). Its contents are solely the responsibility of the authors, and do not necessarily represent the official views of the NIH or the National Eye Institute, which administers this program. BG holds the Erwin Neter Professorial Chair in Cell and Tumor Biology. M. López-García thanks Alexander von Humboldt Foundation for a postdoctoral fellowship. We also like to thank the International Graduate School of Science and Engineering (IGSSE).

## References

- 1. Geiger B, Bershadsky A, Pankov R, Yamada KM. Nature Reviews Molecular Cell Biology. 2001; 2(11):793–805.
- Meyer A, Auernheimer J, Modlinger A, Kessler H. Curr Pharmaceutical Design. 2006; 12(22): 2723–2747.
- 3. Chen CS, Mrksich M, Huang S, Whitesides GM, Ingber DE. Science. 1997; 276(5317):1425–8. [PubMed: 9162012]
- 4. Discher DE, Janmey P, Wang YL. Science. 2005; 310(5751):1139-43. [PubMed: 16293750]
- Arnold M, Cavalcanti-Adam EA, Glass R, Blummel J, Eck W, Kantlehner M, Kessler H, Spatz JP. Chemphyschem. 2004; 5(3):383–8. [PubMed: 15067875]
- 6. Haubner R, Gratias R, Diefenbach B, Goodman SL, Jonczyk A, Kessler H. Journal of the American Chemical Society. 1996; 118(32):7461–7472.
- 7. Cavalcanti-Adam EA, Micoulet A, Blummel J, Auernheimer J, Kessler H, Spatz JP. Eur J Cell Biol. 2006; 85(3–4):219–24. [PubMed: 16546564]
- 8. Cavalcanti-Adam EA, Volberg T, Micoulet A, Kessler H, Geiger B, Spatz JP. Biophys J. 2007; 92(8):2964–74. [PubMed: 17277192]

- 9. Hersel U, Dahmen C, Kessler H. Biomaterials. 2003; 24(24):4385-415. [PubMed: 12922151]
- 10. Plummer ST, Wang Q, Bohn PW, Stockton R, Schwartz MA. Langmuir. 2003; 19(18):7528–7536.
- Kang CE, Gemeinhart EJ, Gemeinhart RA. J Biomed Mater Res A. 2004; 71(3):403–11. [PubMed: 15481057]
- 12. Dertinger SK, Jiang X, Li Z, Murthy VN, Whitesides GM. Proc Natl Acad Sci U S A. 2002; 99(20):12542–7. [PubMed: 12237407]
- 13. Maheshwari G, Brown G, Lauffenburger DA, Wells A, Griffith LG. J Cell Sci. 2000; 113(Pt 10): 1677–86. [PubMed: 10769199]
- 14. Herbert CB, McLernon TL, Hypolite CL, Adams DN, Pikus L, Huang CC, Fields GB, Letourneau PC, Distefano MD, Hu WS. Chemistry & biology. 1997; 4(10):731–7. [PubMed: 9375251]
- 15. Jiang X, Xu Q, Dertinger SKW, Stroock AD, Fu Tm, Whitesides GM. Analytical Chemistry. 2005; 77(8):2338–2347. [PubMed: 15828766]
- Kraus T, Stutz R, Balmer TE, Schmid H, Malaquin L, Spencer ND, Wolf H. Langmuir. 2005;
   21(17):7796–7804. [PubMed: 16089385]
- 17. Lee KB, Park SJ, Mirkin CA, Smith JC, Mrksich M. Science (Washington, DC, United States). 2002; 295(5560):1702–1705.
- 18. Bhat RR, Fischer DA, Genzer J. Langmuir. 2002; 18(15):5640-5643.
- Kramer S, Xie H, Gaff J, Williamson JR, Tkachenko AG, Nouri N, Feldheim DA, Feldheim DL. J Am Chem Soc. 2004; 126(17):5388–95. [PubMed: 15113210]
- 20. Wolfram T, Belz F, Schön T, Spatz JP. Biointerphases. 2006; 2(1):44–48. [PubMed: 20408635]
- 21. Spatz JP, Moessmer S, Hartmann C, Moeller M, Herzog T, Krieger M, Boyen HG, Ziemann P, Kabius B. Langmuir. 2000; 16(2):407–415.
- 22. Glass R, Moeller M, Spatz JP. Nanotechnology. 2003; 14(10):1153–1160.
- 23. Glass R, Arnold M, Bluemmel J, Kueller A, Moeller M, Spatz JP. Advanced Functional Materials. 2003; 13(7):569–575.
- 24. Glass R, Arnold M, Cavalcanti-Adam EA, Blummel J, Haferkemper C, Dodd C, Spatz JP. New Journal of Physics. 2004; 6 No pp given.
- 25. Blümmel J, Perschmann N, Aydin D, Drinjakovic J, Surrey T, López-García M, Kessler H, Spatz JP. Biomaterials. 2007; 94(4):1470–1482.
- 26. Jiang F, Horber H, Howard J, Müller D. J Struct Biol. 2004; 148(3):268-278. [PubMed: 15522775]

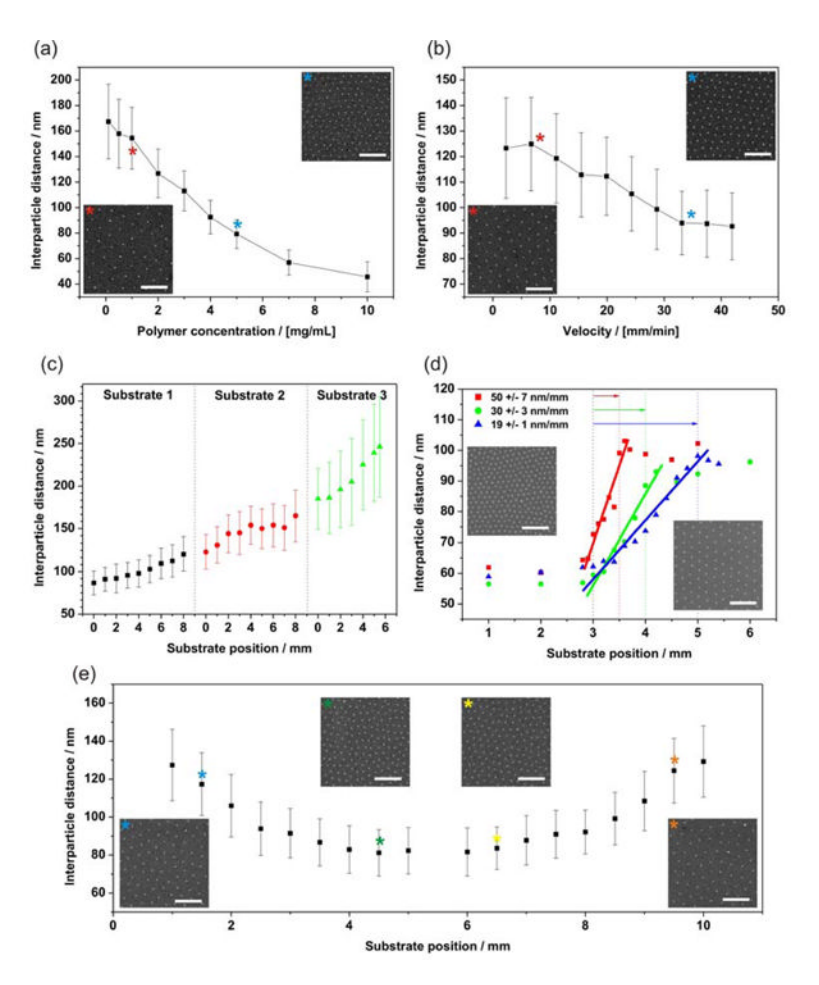


Figure 1. Nanoparticle spacing gradients. Variations in gold nanoparticle spacing along a substrate by using a PS(1780)-b-P[2VP(HAuCl<sub>4</sub>)<sub>0.2</sub>](520) diblock copolymer solution as a function of (a) polymer concentration; substrate retraction velocity (v=12 mm/min), and (b) retraction velocity; polymer solution of 2 mg/mL. (c) Three examples of particle spacing gradients ranging from ~80 to ~250 nm, for three different molecular weight diblock copolymers, and varying substrate retraction velocities [Substrate 1: (PS(990)-b-P[2VP(HAuCl<sub>4</sub>)<sub>0.5</sub>] (385) (c = 3 mg/mL, v = 40 mm/min to 8 mm/min), Substrate 2:  $\bigcirc$  PS(1826)-b- $P[2VP(HAuCl_4)_{0.5}]$  (523) (c = 2 mg/mL, v = 40 mm/min to 8 mm/min) and Substrate 3:  $PS(5355)-b-P[4VP(HAuCl_4)_{0.5}]$  (714) (c = 1 mg/mL, v = 30 mm/min to 8 mm/min)]. (d) Particle spacing gradients with varying gradient strength of (19 +/- 1), (30 +/- 3) and (50 +/-7) nm/mm. Gradients were generated from a PS(990)-b-P[2VP(HAuCl<sub>4</sub>)<sub>0.3</sub>](385) diblock copolymer solution of 5 mg/mL. Retraction procedure: 1) 3 mm constant retraction velocity of 40 mm/min; 2) 0.5, 1 or 2 mm gradual deceleration of retraction velocity from 40 to 8 mm/min; 3) constant retraction velocity of 8 mm/min. All scale bars: 300 nm. Error bars = s.d. of measured particle spacing. (e) Particle spacing for two conversely oriented gradients derived from a PS(1780)-b-P[2VP(HAuCl<sub>4</sub>)<sub>0.2</sub>](520) diblock copolymer solution of 2 mg/ mL on one substrate plotted against substrate position. The retraction velocity was accelerated from 8 to 40 mm/min for the first gradient (0-5 mm) and decreased from 40 to 8 mm/min for the second gradient (6-10 mm) on a single substrate. The asterisks indicate the insets displaying SEM micrographs of the respective substrate positions. Insets show SEM micrographs of the substrate positions indicated by different asterisks (all scale bars: 300 nm)(error bars = Stdev of measured particle spacing).

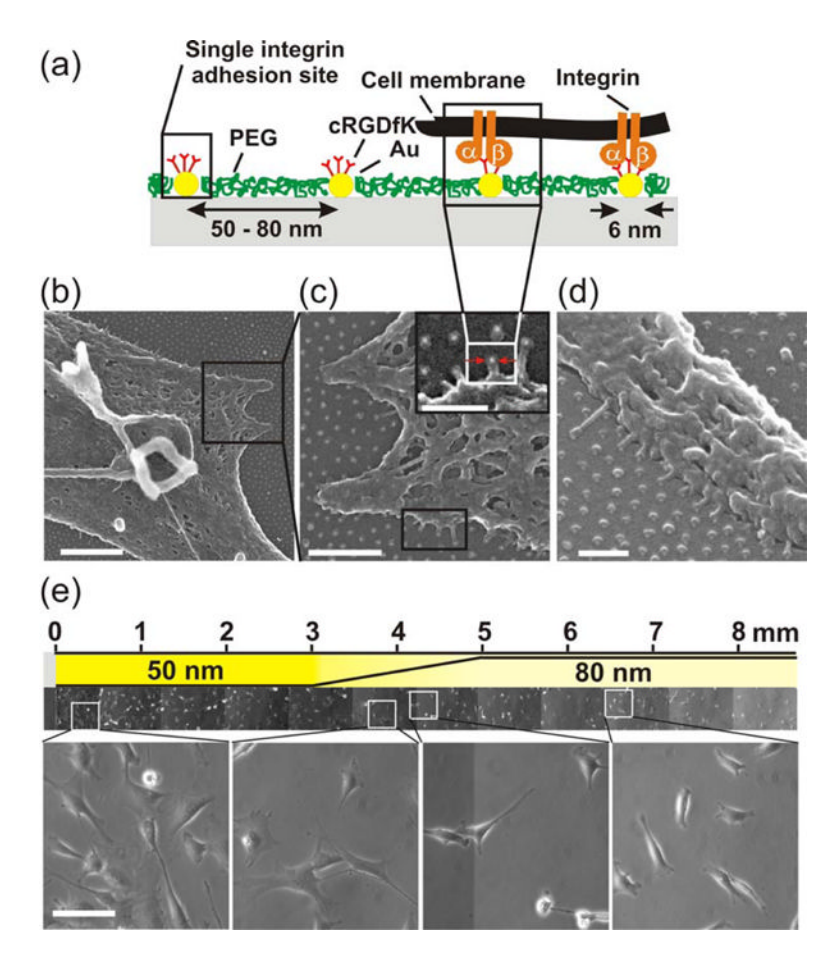


Figure 2. Biofunctionalized particle spacing gradient. (a) Scheme of the biofunctionalized substrate; (b), (c) Scanning electron micrographs show parts of critical point-dried MC3T3 osteoblasts plated for 21 h on biofunctionalized nanopatterns of ~60 nm particle separation. The inset in (c) shows a close-up of ultra-small cellular protrusions with a diameter of ~10 to ~20 nm and a length of ~30 to ~50 nm, interacting selectively with the c(-RGDfK-) functionalized gold nanoparticles which are adhesion patches for single integrin receptors. (d) SE micrograph with a tilt angle of 40° depicts ultra-small cellular protrusions interacting with integrin adhesion sites. (e) Cells were plated for 21 h on biofunctionalized particle spacing gradient substrates with c(-RGDfK-) patch spacing from 50 – 80 nm, between a 3 and 5 mm substrate position. Top: Stitched phase-contrast micrograph presenting the adhesion of cells to the different areas of the substrate. Bottom: Close-up of MC3T3 cells on patch spacing, at substrate areas offering ~50 nm, ~60 nm, ~70 and ~80 nm patch spacing. Scale bars: (b) 500 nm; (c) 200 nm (Inset: 100 nm); (d) 100 nm; (e) 100 μm.

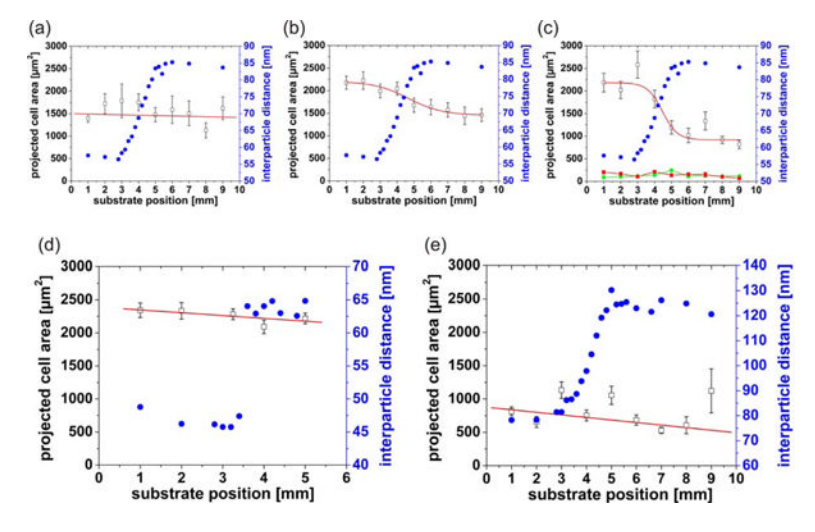


Figure 3.
Projected area of cells adhering along gradients covering various ligand patch spacing, strengths, and adhesion times. Ligand patch spacing ( ●) and projected cell area ( ) of cells plated after (a) 2.5 h (248 cells analysed); (b) 8 h (159 cells analysed); and (c) 23 h (200 cells analysed) as a function of substrate position, with a gradient strength of 15 nm/mm each. Control experiments with non-functionalized nanogold particles ( ■) and particle that were functionalized with RGE-peptides ( ●) proved the specificity of cell responses due to c(-RGDfK-) functionalization. Also the total number of cells that could be detected on the substrate with these controls was very little, i.e. couple of tens. Ligand patch spacing ( ●) and projected cell area ( ) 23 h after cell plating as a function of substrate position, when the spacing range of c(-RGDfK-) patches covers (d) 45-65 nm, gradient strength 80 nm/mm; and (e) 80-110 nm, gradient strength 15 nm/mm.

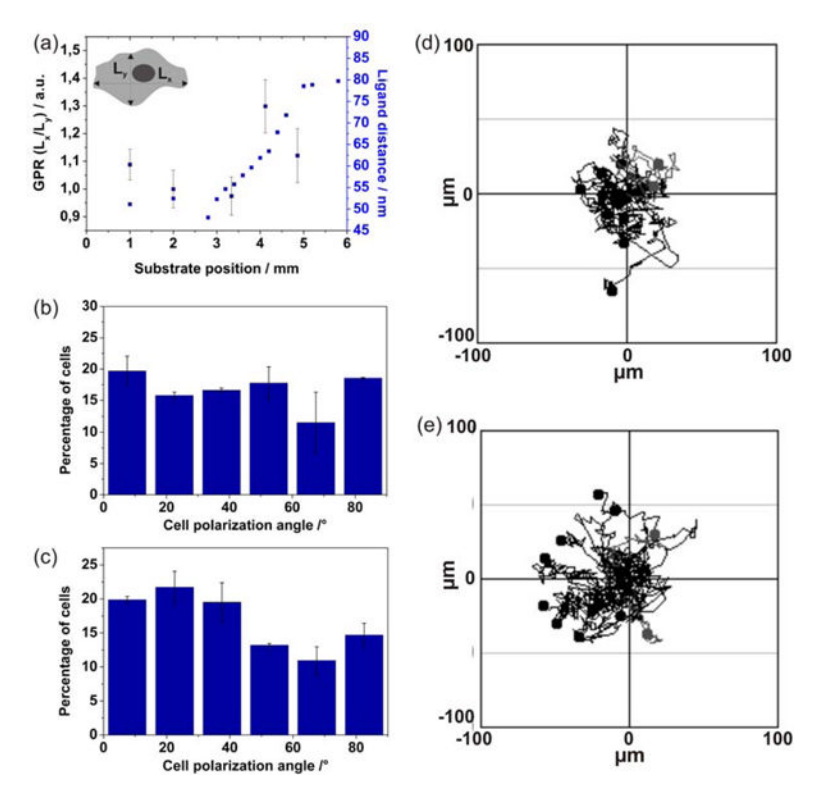


Figure 4.

Morphological analysis of MC3T3 osteoblasts in contact with ligand patch spacing gradients. (a) GPR-value ( ) and ligand patch spacing ( □) as a function of substrate position for cells adhering to a gradient with a strength of 15 nm/mm. Cell polarization angle distribution of MC3T3 osteoblasts adhering to areas which consist of (b) a constant ligand patch spacing of ~50 nm and (c) a gradient as documented in (a) (0° = cells oriented along the gradient; 90° = cells oriented perpendicular to the gradient). REF fibroblast migration paths on areas which present (d) a constant ligand patch spacing of ~60 nm; and (e) a ligand patch gradient with a strength of 25 nm/mm covering 60 to 110 nm spacing. For migration studies cells were cultured for 13 h on the respective substrates and then imaged every 10 min. for 12 h.